Magnetic flux disorder and superconductor-insulator transition in nanohole thin films

Enzo Granato

Laboratório Associado de Sensores e Materiais, Instituto Nacional de Pesquisas Espaciais, 12227-010 São José dos Campos, SP, Brazil

We study the superconductor-insulator transition in nanohole ultrathin films in a transverse magnetic field by numerical simulation of a Josephson-junction array model. Geometrical disorder due to the random location of nanoholes in the film corresponds to random flux in the array model. Monte Carlo simulation in the path-integral representation is used to determine the critical behavior and the universal resistivity at the transition as a function of disorder and average number of flux quanta per cell, f_o. The resistivity increases with disorder for noninteger f_o while it decreases for integer f_o, and reaches a common constant value in a vortex-glass regime above a critical value of the flux disorder D_f^c. The estimate of D_f^c and the resistivity increase for noninteger f_o are consistent with recent experiments on ultrathin superconducting films with positional disordered nanoholes.

There is growing interest in the superconductor-insulator (SI) transition in ultrathin films with a lattice of nanoholes [1–6]. This system is an important testing ground for models of the universality class of the quantum phase transition since the patterned nanostructure provides a sensitive probe for distinguishing between phase and amplitude fluctuations of the superconducting order parameter. The magnetoresistance oscillatory behavior at low magnetic fields near the transition is analogous to the one observed in microfabricated Josephson-junction arrays, which undergo a SI transition due to the small electrical capacitance of the superconducting grains [7–11]. This common feature results from phase-coherence effects, which can be described by the same generic model of phase fluctuations of the superconducting order parameter, a Josephson-junction array model, with a wider applicability. In fact, it is closely related to the Bose-Hubbard model, where Cooper pairs interact on a lattice potential, in the limit of a large number of bosons per site [8,12], to the quantum rotor model [12–14], and to ultracold atoms on optical lattices [15–17]. For a periodic nanohole film at low magnetic fields, the simplest model consists of a frustrated array of superconducting "grains", where the phase is well defined locally, coupled by Josephson junctions or weak links on a periodic lattice, with the lattice of nanoholes corresponding to the dual lattice, which acts as a vortex pinning center [18,19]. The number of flux quanta per unit cell of the nanohole lattice, which is proportional to the external magnetic field, corresponds to the frustration parameter f of the Josephson-junction array model. The zero-temperature quantum phase transition in the array model, driven by the competition between the charging energy and Josephson-coupling energy at different frustration parameters, corresponds to the SI transition in the nanohole film in the external magnetic field. The resistivity at the transition is expected to be finite and universal [12,13,20,21], depending only on the universality class of the transition, which generally changes in the presence of a magnetic field and disorder.

Very recently, intriguing experimental results have been obtained near the SI transition in thin films with a disordered triangular lattice of nanoholes with a controlled amount of positional disorder [5,6]. Such disorder leads to spatial variations in the magnetic flux per unit cell, which increases with the magnetic field, similar to the effects of geometrical

disorder in microfabricated Josephson-junction arrays [22,23]. Magnetoresistance oscillations decrease in amplitude and disappear above a critical value of flux disorder. However, the resistivity at successive field-induced transitions *increases* with flux disorder, in apparent disagreement with predictions of universality [12,13,20] and a previous numerical simulation [24], which show a *decrease* of the resistivity.

In this Rapid Communication, we study the SI transition in geometrically disordered nanohole thin films by numerical simulation of a Josephson-junction array model with flux disorder. Geometrical disorder due to the random locations of nanoholes in the film corresponds to random flux in the array model. Monte Carlo (MC) simulation in the path-integral representation is used to determine the critical behavior and the resistivity at the transition as a function of flux-disorder strength D_f and average number of flux quanta per cell, f_o. It is found that the resistivity at the transition increases with disorder for noninteger f_o while it decreases for integer f_o, and reaches an approximately common constant value in a vortex-glass regime above a critical value D_f^c. The distinct behavior for noninteger f_o results from the interplay of vortex-lattice commensurability and flux-disorder effects. The estimate of D_f^c and the resistivity increase for noninteger f_o are in good agreement with available experimental data on positional disordered nanohole thin films [5] for noninteger f_o while it calls for further measurements for integer f_o.

We consider a Josephson-junction array model, which allows for both flux-disorder and charging effects [7,22,24], described by the Hamiltonian

$$\mathcal{H} = -\frac{E_c}{2} \sum_i n_i^2 - \sum_{\langle ij \rangle} E_{ij} \cos\left(\theta_i - \theta_j - A_{ij}^o - t_{ij}\right). \quad (1)$$

The first term in Eq. (1) describes quantum fluctuations induced by the charging energy, $E_c n_i^2/2$, of a non-neutral superconducting grain located at site i of a periodic reference lattice, where $E_c = 4e^2/C$, e is the electronic charge, and $n_i = -i\partial/\partial\theta_i$ is the operator, canonically conjugate to the phase operator θ_i, representing the deviation of the number of Cooper pairs from a constant integer value. The effective capacitance to the ground of each grain C is assumed to be spatially uniform, for simplicity. The second term in (1) is the Josephson-junction coupling between nearest-neighbor

grains described by phase variables θ_i. The effect of the magnetic field **B** applied in the perpendicular ($\hat{z}$ direction) appears through the link variables A_{ij}^o and t_{ij}, which satisfy the constraints $\sum_{ij} A_{ij}^o = 2\pi f_o$ and $\sum_{ij} t_{ij} = 2\pi \delta f_p$, where the gauge-invariant sums $\sum_{ij}$ are over the links ij surrounding the site p of the plaquette centers. f_o is a uniform constant parameter and δf_p is a spatially varying random variable with zero average. The effects of the positional disorder of the nanoholes, which correspond to random plaquette areas S_p of the array, can be incorporated in this model by identifying f_o as the average number of flux quanta per plaquette $B S_o/\Phi_o$, where $\Phi_o = hc/2e$ is the flux quantum, and S_o as the uniform plaquette area of the reference lattice. δf_p then represents the additional random flux $f_o \delta S_p / S_o$, where $\delta S_p = S_p - S_o$. Previous work on the SI transition [24] studied this model defined on a square lattice for integer f_o and uncorrelated disorder in t_{ij}. In order to compare with available experimental data for superconducting films with a triangular lattice of nanoholes in the weak disorder limit [1,5], we consider here the array model defined on a honeycomb lattice [25] and take δf_p as an uncorrelated random variable. For convenience, we use a uniform disorder distribution $\delta f_p = D_f[-1,1]$, with the random-flux-disorder strength $D_f = f_o D_a$, where D_a measures the disorder in the areas $\delta S_p / S_o$. Experimentally, the flux disorder D_f can be varied by changing f_o via the external field or the geometrical disorder D_a using different samples [5]. We also allow for bond disorder in the form of random Josephson couplings [26] $E_{ij} = E_J e_{ij}$, where $e_{ij} = 1 \pm D_b$ with equal probability and disorder parameter strength D_b. In the numerical simulations described below we set $D_b = 0.3$, but its value does not change the main results. With this choice the magnetoresistance behavior of films with a triangular lattice of nanoholes without flux disorder [1,4] can already be described by the array model [18,19]. Here we consider the effects of increasing the flux disorder D_f for integer $f_o = n$ and noninteger rational values $f_o = n + 1/q$ of the frustration parameter.

To study the quantum phase transition at zero temperature, we employ the imaginary-time path-integral formulation of the model [8]. In this representation, the two-dimensional (2D) quantum model of Eq. (1) maps into a (2+1)D classical statistical mechanics problem. The extra dimension corresponds to the imaginary-time direction. The classical reduced Hamiltonian can be written as

$$H = -\frac{1}{g}\left[\sum_{\tau,i} \cos(\theta_{\tau,i} - \theta_{\tau+1,i})\right.$$
$$\left. + \sum_{\langle ij \rangle, \tau} e_{ij} \cos\left(\theta_{\tau,i} - \theta_{\tau,j} - A_{ij}^o - t_{ij}\right)\right], \quad (2)$$

where $e_{ij} = E_{ij}/E_J$ and τ labels the sites in the discrete time direction. The ratio $g = (E_c/E_J)^{1/2}$, which drives the SI transition for the model of Eq. (1), corresponds to an effective "temperature" in the 3D classical model of Eq. (2). In general, a quantum phase transition shows intrinsic anisotropic scaling, with different diverging correlation lengths ξ and ξ_τ in the spatial and imaginary-time directions [8], respectively, related by the dynamic critical exponent z as $\xi_\tau \propto \xi^z$. The classical

Hamiltonian of Eq. (2) can be viewed as an XY model on a layered honeycomb lattice, where frustration effects exist only in the honeycomb layers. Randomness in e_{ij} and t_{ij} corresponds to disorder completely correlated in the time direction. The honeycomb lattice is defined on a rectangular geometry with linear size given by a dimensionless length L. In terms of L, the linear sizes in the $\hat{x}$ and $\hat{y}$ directions correspond to $L_x = L\sqrt{3}/2$ and $L_y = \frac{3}{2}L$, respectively. We choose a gauge where $A_{ij} = 2\pi f n_y$, on alternating (tilted) bonds along the rows in the $\hat{x}$ direction numbered by the integer n_y and $A_{ij} = 0$ otherwise.

Equilibrium MC simulations for $E_c > 0$ are carried out using the 3D classical Hamiltonian in Eq. (2) regarding g as a "temperature"-like parameter. The parallel tempering method [27] is used in the simulations with periodic boundary conditions, as in previous work [19]. The finite-size scaling analysis is performed for different sizes L with the constraint $L_\tau = aL^z$, where a is a constant aspect ratio. This choice simplifies the scaling analysis, otherwise an additional scaling variable L_τ/L^z would be required to describe the scaling functions. The value of a is chosen to minimize the deviations of aL^z from integer numbers. However, this requires one to know the value of the dynamic exponent z in advance. Since the exact value of z is not known, we follow a two-step approach. First, we obtain an estimate of g_c and z from simulations performed with a *driven* MC dynamics method, which has been used in the context of the 3D XY-spin glass model [28]. Then, these initial estimates are improved by finding the best data collapse for the finite-size behavior of the phase stiffness in the time direction γ_τ, obtained by the equilibrium MC method. For the driven MC method, the layered honeycomb model of Eq. (2) is viewed as a 3D superconductor and the corresponding "current-voltage" scaling near the transition is used to determine the critical coupling and critical exponents [29]. In the presence of an external driving perturbation J_x ("current density") which couples to the phase difference $\theta_{\tau,i+\hat{x}} - \theta_{\tau,i}$ along the $\hat{x}$ direction, the classical Hamiltonian of Eq. (2) is modified to

$$H_J = H - \sum_{i,\tau} J_x(\theta_{\tau,i+\hat{x}} - \theta_{\tau,i}). \quad (3)$$

When $J_x \neq 0$, the system is out of equilibrium since the total energy is unbounded. The lower-energy minima occur at phase differences $\theta_{\tau,i+\hat{x}} - \theta_{\tau,i}$, which increase with time t, leading to a net phase slippage rate proportional to $V_x = \langle d(\theta_{\tau,i+\hat{x}} - \theta_{\tau,i})/dt \rangle$, corresponding to the average "voltage" per unit length. The MC simulations are carried out using the Metropolis algorithm, and the time dependence is obtained by identifying the time t as the MC time. The measurable quantity of interest is the phase slippage response ("nonlinear resistivity") defined as $R_x = V_x/J_x$. Similarly, we define R_τ as the phase slippage response to the applied perturbation J_τ in the layered (imaginary-time) direction. Above the phase-coherence transition, $g > g_c$, R_x should approach a nonzero value when $J_x \to 0$ while it should approach zero below the transition. From the nonlinear scaling behavior near the transition of a sufficiently large system, one can extract the critical coupling g_c, and the critical exponents ν and z. In the absence of charging effects, R_x remains zero below
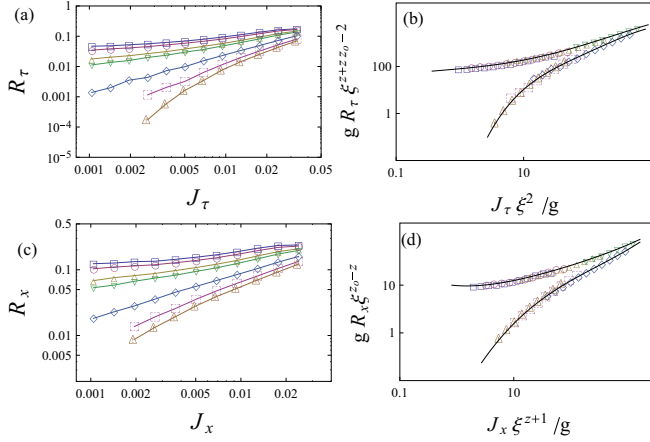
FIG. 1. Phase slippage response in (a) the imaginary-time direction R_τ and (c) spatial direction R_x for $f_o = n + 1/6$, near the transition. Flux-disorder strength $D_f = 0.7$ and system size $L = 60$. The couplings g from the top down are 1.48, 1.47, 1.45, 1.44, 1.41, 1.39, and 1.38. (b) and (d) Scaling plots corresponding to (a) and (c), respectively, for data near the transition with $\xi = |g/g_c - 1|^{-\nu}$ and the same parameters $g_c = 1.426$, $z_0 = 2.3$, $z = 1.2$, and $\nu = 1.1$.

a critical value $J_x = J_c$, which provides an estimate of the critical current for the model of Eq. (1), when $E_c = 0$.

We show in detail the results for $f_o = n + 1/6$ and $D_f = 0.7$. This value of frustration was chosen to allow a comparison with the available experimental data [5]. Figure 1 shows the behavior of the nonlinear phase slippage response R_x and R_τ as a function of the applied perturbation J_x and J_τ, respectively, for different couplings g and large system size. The behavior is consistent with a phase-coherence transition at an apparent critical coupling in the range $g_c \sim 1.41$–1.44. For $g > g_c$, both R_x and R_τ tend to a finite value, while for $g < g_c$ they extrapolate to low values. The critical coupling g_c and critical exponents ν and z can then be obtained from the best data collapse satisfying the scaling behavior close to the transition. The required scaling theory is described in detail in Ref. [30]. R_x and R_τ should satisfy the scaling forms

$$g R_x \xi^{z_0 - z} = F_\pm(J_x \xi^{z+1}/g),$$
$$g R_\tau \xi^{z + z_0 z - 2} = H_\pm(J_\tau \xi^2/g),$$

where z_0 is an additional critical exponent describing the MC relaxation times, $t_x \sim \xi^{z_0}$ and $t_\tau \sim \xi_\tau^{z_0}$, in the spatial and imaginary-time directions, respectively, and $\xi = |g/g_c - 1|^{-\nu}$. The + and − signs correspond to $g > g_c$ and $g < g_c$, respectively. The two scaling forms are the same when $z = 1$, corresponding to isotropic scaling. The joint scaling plots according to Eqs. (4) are shown in Fig. 1, obtained by adjusting the unknown parameters, providing the estimates $g_c = 1.426$, $z_0 = 2.3$, $z = 1.2$, and $\nu = 1.1$.

The above estimate of g_c and z does not take into account the finite-size effects. It assumes that the system is sufficient large and the coupling is not too close to g_c such that the correlation length is smaller than the system size. To improve these estimates we consider the finite-size behavior of the phase stiffness in the imaginary-time direction γ_τ. The phase stiffness γ_τ, which is a measure of the free energy cost to
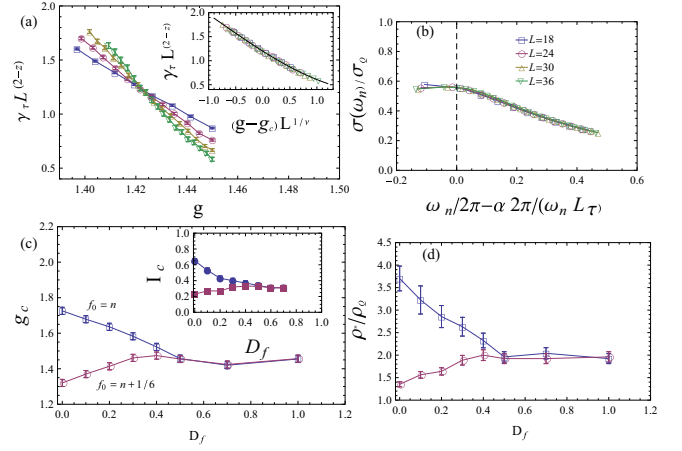

FIG. 2. (a) Phase stiffness in the imaginary-time direction γ_τ for different system sizes L, near the transition point estimated from Fig. 1. $L_\tau = aL^z$, with aspect ratio $a = 0.628$ and $z = 1.25$. Inset: Scaling plot of γ_τ with $g_c = 1.424$ and $\nu = 0.97$. (b) Scaling plot of conductivity $\sigma(iw_n)$ at the critical coupling g_c with $\alpha = 0.15$. The universal conductivity is given by the intercept with the $x = 0$ dashed line, leading to $\frac{\sigma^*}{\sigma_Q} = 0.56(3)$. (c) Critical coupling g_c at different values of the average frustration f_o and increasing flux-disorder strength D_f. Inset: Behavior of the corresponding critical currents I_c at $E_c = 0$. (d) Resistivity $\rho^* = 1/\sigma^*$ in units of $\rho_Q = 1/\sigma_Q$ at the transition for the different average frustrations indicated in (c) and increasing flux disorder D_f.

impose an infinitesimal phase twist in the time direction, is given by [13]

$$\gamma_\tau = \frac{1}{L^3 g^2}\big[g\langle\epsilon_\tau\rangle - \langle I_\tau^2\rangle + \langle I_\tau\rangle^2\big]_D,$$ (5)

where $\epsilon_\tau = \sum_{\tau,i}\cos(\theta_{\tau,i} - \theta_{\tau+1,i})$ and $I_\tau = \sum_{\tau,i}\sin(\theta_{\tau,i} - \theta_{\tau+1,i})$. In Eq. (5), $\langle\cdots\rangle$ represents a MC average for a fixed disorder configuration and $[\cdots]_D$ represents an average over different disorder configurations. In the superconducting phase γ_τ should be finite, reflecting the existence of phase coherence, while in the insulating phase it should vanish in the thermodynamic limit. For a continuous phase transition, γ_τ should satisfy the finite-size scaling form

$$\gamma_\tau L^{2-z} = F(L^{1/\nu}\delta g),$$ (6)

where $F(x)$ is a scaling function and $\delta g = g - g_c$. This scaling form implies that data for $\gamma_\tau L^{2-z}$ as a function of g, for different system sizes L, should cross at the critical coupling g_c. Figure 2(a) shows this crossing behavior obtained near the initial estimate of g_c by varying z slightly from its initial value. In the inset of this figure, we show a scaling plot of the data according to the scaling form of Eq. (6), which provides the final estimates $g_c = 1.424$ and $\nu = 0.97$.

We have also determined the universal conductivity at the critical point from the frequency and finite-size dependence of the phase stiffness $\gamma(w)$ in the spatial direction, following the scaling method described by Cha *et al.* [12,13]. The conductivity is given by the Kubo formula

$$\sigma = 2\pi\sigma_Q \lim_{w_n \to 0} \frac{\gamma(iw_n)}{w_n},$$ (7)

where $\sigma_Q = (2e)^2/h$ is the quantum of conductance and $\gamma(iw_n)$ is a frequency-dependent phase stiffness evaluated at the finite frequency $w_n = 2\pi n/L_\tau$, with n an integer. The phase stiffness in the $\hat{x}$ direction is given by

$$\gamma = C[g\langle\epsilon_x\rangle - \langle|I(iw_n)|^2\rangle + \langle|I(iw_n)|\rangle^2]_D, \qquad (8)$$

where $C = 1/[(4/3\sqrt{3})NL_\tau g^2]$, N is the total number of sites in each layer,

$$\epsilon_x = \sum_{\tau,j}(\hat{x}\cdot\hat{u}_{j,j+\hat{x}})^2 e_{i,j+\hat{x}}\cos(\Delta_x\theta_{\tau,j}),$$

$$I(iw_n) = \sum_{\tau,j}(\hat{x}\cdot\hat{u}_{j,j+\hat{x}})e_{i,j+\hat{x}}\sin(\Delta_x\theta_{\tau,j})e^{iw_n\tau}, \qquad (9)$$

$\hat{u}_{j,j+\hat{x}}$ is a unit vector between nearest-neighbor sites and $\Delta_x\theta_{\tau,j} = \theta_{\tau,j} - \theta_{\tau,j+\hat{x}} - A^o_{j,j+\hat{x}} - t_{j,j+\hat{x}}$. At the transition, $\gamma(iw_n)$ vanishes linearly with frequency and σ assumes a universal value σ^*, which can be extracted from its frequency and finite-size dependence [13]

$$\frac{\sigma(iw_n)}{\sigma_Q} = \frac{\sigma^*}{\sigma_Q} - c\left(\frac{w_n}{2\pi} - \alpha\frac{2\pi}{w_nL_\tau}\right)\cdots. \qquad (10)$$

The parameter α is determined from the best data collapse of the frequency-dependent curves for different systems sizes in a plot of $\frac{\sigma(iw_n)}{\sigma_Q}$ vs $x = (\frac{w_n}{2\pi} - \alpha\frac{2\pi}{w_nL_\tau})$. The universal conductivity is obtained from the intercept of these curves with the line $x = 0$. The calculations were performed for different system sizes with $L_\tau = aL^z$, using the above estimates of z and g_c. From the scaling behavior in Fig. 2(b) we obtain $\sigma^*/\sigma_Q = 0.56(3)$, where the estimated uncertainly is mainly the result of the error in the coupling g_c.

We have performed extensive calculations as a function of the flux-disorder strength D_f for integer $f_o = n$ and noninteger $f_o = n + 1/6$. The behavior of the critical couplings g_c for the SI transition as a function of D_f is shown in Fig. 2(c) and the corresponding behavior of the resistivity at the transition $\rho^* = 1/\sigma^*$ is shown in Fig. 2(d). Disorder changes significantly the values of the critical coupling and resistivity for small D_f while they remain essentially unchanged and frustration independent above a critical value $D_f^c \sim 0.5$. Below D_f^c, the resistivity at the transition increases with disorder for noninteger f_o but it decreases for integer f_o. This critical disorder D_f^c should correspond to a transition into a vortex-glass regime, where one expects that g_c should be insensitive to the value of the frustration. Similar behavior is also expected for the critical current in absence of charging effects [31]. Calculations for the critical current for the model of Eq. (1) with $E_c = 0$ using the driven MC dynamics are shown in the inset of Fig. 2(c). The transition from a low-disorder regime, where the critical current is sensitive to frustration, to a glassy regime occurs at approximately the same critical value D_f^c.

The results for noninteger f_o are in good agreement with available experimental observations on ultrathin superconducting films with positional disordered nanoholes [5]. As in other calculations of the resistivity at the transition [11–13,17,19], the obtained value differs significantly from the experimental value. However, the trend as a function of disorder and the magnetic field dependence should be

consistent with experiments. In fact, the resistivity for large flux disorder found experimentally for the field-induced SI transition in nanohole films [5] is a factor of 1.8(2) higher than in the absence of disorder, which agrees reasonably well with our numerical estimate of 1.5(3) for noninteger f_o in Fig. 2(d). The experimental data also allow a rough estimate of the critical exponent product $z\nu \sim 1.4(4)$, from the expected scaling behavior of the resistivity derivative at the transition [21] as a function of temperature T, $\partial\rho/\partial B \propto T^{-1/(z\nu)}$. Our numerical estimate $z\nu = 1.21(5)$ is compatible with the experimental value, although the error bars are large. Moreover, the critical disorder strength below which magnetoresistance oscillations are observed experimentally [5], $\delta f_c \sim 0.3$, can also be compared with the critical disorder strength $D_f^c \sim 0.5$ found numerically. These oscillations occur below D_f^c, where the critical coupling for the SI transition g_c in Fig. 2(c) is sensitive to frustration, with decreasing amplitude as the flux disorder $D_f = f_oD_g$ approaches D_f^c for increasing frustration. Since in the present calculations δf is uniformly distributed, rather than approximately Gaussian distributed as in the experiments, a conversion factor is required for comparing the critical values. Requiring the variance of both distributions to be the same leads to an equivalent flux-disorder strength $\sim 0.5/\sqrt{3} = 0.29$, which is in reasonable agreement with the experimental value. For integer f_o, the resistivity in Fig. 2(d) for large flux disorder decreases by a factor of 1.7(3). A much larger decrease has been found previously [24] for the model of Eq. (1) defined on a square lattice with uncorrelated disorder in t_{ij}. Unfortunately, experimental data for integer f_o, including $f_o = 0$, on the same sample are not available yet to make a comparison to the numerical results. However, the resistivity found in recent experiments for larger flux disorder [6] decreases by a factor ~ 2 compared with earlier measurements on samples without flux disorder [1], which is compatible with the present calculations.

The change of the resistivity and the different behavior for noninteger f_o as a function of D_f can be understood as the interplay of vortex-lattice commensurability and flux-disorder effects. In absence of disorder, the SI transition for noninteger f_o is in a different universality class from the zero field case [11]. The net circulating currents around each plaquette, introduced by the external field, correspond to a pinned commensurate vortex lattice which changes the ground-state symmetry. Since the resistivity depends on the universality class [20], its value for noninteger f_o can be significantly different. For $f_o = 1/2$ on a square lattice [10,11,13,17], for example, it decreases by a factor of 2. In the present case of a honeycomb lattice, the SI transition for $f_o = 1/2$ is yet in another universality class different from the square lattice [19], and the resistivity decreases by a factor of approximately 4. On the other hand, for large flux disorder, where there is a vortex-glass phase for both integer and noninteger f_o, the universality and the resistivity should be the same, since the vortices are in a highly disordered configuration.

In conclusion, we found that the resistivity at the SI transition increases with magnetic-flux disorder D_f for noninteger frustration f_o while it decreases for integer f_o, and reaches an approximately common value in a vortex-glass regime for $D_f > D_f^c$. In the simplest scenario, one expects different critical behavior for weak and strong disorder. Although

the obtained constant value of the resistivity for $D_f > D_f^c$ indicates universal behavior in a different universality class, the variation of the resistivity for small disorder, however, may be a result of crossover effects due the limited system sizes. In the experiments, temperatures not sufficiently low should have similar effects. In the absence of such effects, the results cannot rule out a truly nonuniversal behavior. The results could also be tested experimentally in microfabricated Josephson-junction arrays with controlled parameters. How- ever, for a more realistic description of these systems, disorder from offset charges and dissipation effects [7], which have been neglected in the present model, should be taken into account.

[1] M. D. Stewart, Jr., A. Yin, J. M. Xu, and J. M. Valles, Jr., Science **318**, 1273 (2007).

[2] M. D. Stewart, Jr., A. Yin, J. M. Xu, and J. M. Valles, Jr., Phys. Rev. B **77**, 140501 (2008).

[3] T. I. Baturina, V. M. Vinokur, A. Yu. Mironov, N. M. Chtchelkatchev, D. A. Nasimov, and A. V. Latyshev, Europhys. Lett. **93**, 47002 (2011).

[4] G. Kopnov, O. Cohen, M. Ovadia, K. H. Lee, C. C. Wong, and D. Shahar, Phys. Rev. Lett. **109**, 167002 (2012).

[5] H. Q. Nguyen, S. M. Hollen, J. M. Valles, Jr., J. Shainline, and J. M. Xu, Phys. Rev. B **92**, 140501 (2015).

[6] H. Q. Nguyen, S. M. Hollen, J. M. Valles, Jr., J. Shainline, and J. M. Xu, arXiv:1511.08135.

[7] R. Fazio and H. van der Zant, Phys. Rep. **355**, 235 (2001).

[8] S. L. Sondhi *et al.*, Rev. Mod. Phys. **69**, 315 (1997).

[9] L. J. Geerligs, M. Peters, L. E. M. de Groot, A. Verbruggen, and J. E. Mooij, Phys. Rev. Lett. **63**, 326 (1989).

[10] H. S. J. van der Zant, L. J. Geerligs, and J. E. Mooij, Europhys. Lett. **19**, 541 (1992).

[11] E. Granato and J. M. Kosterlitz, Phys. Rev. Lett. **65**, 1267 (1990).

[12] M.-C. Cha, M. P. A. Fisher, S. M. Girvin, M. Wallin, and A. P. Young, Phys. Rev. B **44**, 6883 (1991).

[13] M.-C. Cha and S. M. Girvin, Phys. Rev. B **49**, 9794 (1994).

[14] T. K. Kopec and T. P. Polak, Phys. Rev. B **66**, 094517 (2002).

[15] T. P. Polak and T. K. Kopec, Phys. Rev. A **79**, 063629 (2009).

[16] M. Atala *et al.*, Nat. Phys. **10**, 588 (2014).

[17] A. S. Sajna, T. P. Polak, and R. Micnas, Phys. Rev. A **89**, 023631 (2014).

[18] E. Granato, Phys. Rev. B **87**, 094517 (2013).

[19] E. Granato, Eur. Phys. J. B **89**, 68 (2016); J. Phys.: Conf. Ser. **568**, 022017 (2014).

[20] M. P. A. Fisher, G. Grinstein, and S. M. Girvin, Phys. Rev. Lett. **64**, 587 (1990).

[21] M. P. A. Fisher, Phys. Rev. Lett. **65**, 923 (1990).

[22] E. Granato and J. M. Kosterlitz, Phys. Rev. B **33**, 6533 (1986); Phys. Rev. Lett. **62**, 823 (1989).

[23] M. G. Forrester, H. J. Lee, M. Tinkham, and C. J. Lobb, Phys. Rev. B **37**, 5966 (1988); S. P. Benz, M. G. Forrester, M. Tinkham, and C. J. Lobb, *ibid.* **38**, 2869 (1988).

[24] K. Kim and D. Stroud, Phys. Rev. B **78**, 174517 (2008).

[25] The charging energy E_c of such an array, associated with a node of the nanohole film, was estimated to be too large [1,2]. However, in the present model, it is an effective parameter, which incorporates other effects, leading to E_c comparable to E_J.

[26] Bond disorder washes out the secondary minimum at $f = 1/3$ predicted by the model for the magnetoresistance oscillations [18,19] when $D_f = 0$, leading to a behavior consistent with experiments [1,4]. It is also generated by the random nanohole positions without coupling to the external field.

[27] K. Hukushima and K. Nemoto, J. Phys. Soc. Jpn. **65**, 1604 (1996).

[28] E. Granato, Phys. Rev. B **69**, 144203 (2004).

[29] C. Wengel and A. P. Young, Phys. Rev. B **56**, 5918 (1997).

[30] K. H. Lee, D. Stroud, and S. M. Girvin, Phys. Rev. B **48**, 1233 (1993).

[31] E. Granato and D. Domínguez, Phys. Rev. B **63**, 094507 (2001).